

Light control through scattering media with neural networks

Alex Turpin, Ivan Vishniakou, and Johannes D. Seelig*
Center of Advanced European Studies and Research, 53175 Bonn, Germany
(Dated: December 14, 2024)

Scattering often limits the controlled delivery of light in applications such as biomedical imaging [1–3], optogenetics [4], optical trapping [5], and fiber-optic communication and imaging [6, 7]. Recent work has shown that this limit can be overcome by adapting the light wavefront entering the scattering material, either iteratively to achieve a predefined light distribution [8–10] or using phase sensitive methods to achieve deterministic light control simultaneously across an entire field of view [11–13]. Here, we demonstrate a machine-learning approach requiring only intensity projections and measurements for achieving light control through scattering media. Using pairs of binary intensity patterns and intensity measurements we train neural networks (NNs) to provide the modulating patterns necessary to control the shape of the beam after the scatterer. Our approach demonstrates the usefulness of machine-learning techniques, and in particular NNs, for high-resolution point spread function (PSF) engineering in scattering materials and suggests that NNs will find applications to efficiently and flexibly correct for scattering in optical imaging and light delivery.

When light propagates through a linear non-homogeneous and non-isotropic material its wavefront becomes distorted due to aberrations and scattering, resulting in an apparently random interference pattern of granular speckles [3]. Such scattering conditions hamper the controlled delivery of light and the engineering of the PSF, which is a basic requirement for many applications. To counteract this effect, methods based on shaping the light wavefront entering the scattering material have been developed. Wavefront shaping is typically achieved by using spatial light modulators (SLMs) [14, 15] which, with their millions of degrees of freedom (pixels), allow focusing through diffusers [8, 11], multi-mode fibers [6, 12, 16, 17], and biological tissue [4, 18–20]. Different techniques have been developed to determine the appropriate wavefront corrections to be displayed on the SLM. For example, digital optical phase conjugation uses interferometry to measure the scattered light field and reverses it with an SLM [19, 21–24]. This technique has the advantage of achieving very high update rates, approaching the millisecond range needed for imaging in dynamic biological tissue [25], while however

requiring that the scattering signal originates from a coherent source suitable for reversal. Alternatively, algorithms that iteratively optimize the light phase or intensity depending on the resulting scattered light distribution (typically aiming for a single focal spot) can also compensate for scattering [5, 8, 9, 26, 27]. Such feedback-based algorithms require that the optimization process repeats each time the desired position or shape of the focus is changed, although, at least in some applications, this has been achieved at very high rates [28]. Other approaches are based on a transmission matrix that describes the scattering process across an entire field of view [6, 11, 12, 29] and thus allows the control of light after the scatter [30]. For obtaining the transmission matrix, one needs to measure the light phase, which, similar to digital optical phase conjugation, requires technically demanding interferometric approaches.

To simplify such experiments, several of these approaches have also been complemented with computational methods for estimating incompletely measured information, for example inferring the light phase from intensity measurements [13, 31]. Another set of computational techniques that, thanks to the development of programming frameworks together with the computational power of GPUs, is increasingly being applied in imaging and microscopy relies on machine learning (ML) [32–35] and in particular on NNs [36–39]. The usefulness of these techniques has been demonstrated in the context of light scattering [40–47], however, mostly for image analysis [37, 44, 45, 47], where the goal typically lies in the classification of an object across a scattering layer or image reconstruction based on a predefined data set [48]. For light control, genetic algorithms, a class of iterative optimization algorithms, have been successfully used for focusing across scattering materials and, in some cases, shown improved performance over non-genetic iterative alternatives [40–43]. Single- and multi-focus single-shot control (after training) over a 5×5 pixel area has been achieved using support vector regression [46], but the reported small field of view, limited signal to noise ratio, and long training times (97 min) are currently limiting for high-resolution PSF engineering. Overall, approaches for single-shot PSF control using machine learning have so far fallen short of the performance of transmission-matrix approaches.

Here we show that single-layer NNs (SLNNs) and multi-layer convolutional NNs (CNNs) can be trained to predict the illumination patterns necessary for controlling the light distribution behind a scattering material with high accuracy. Our method does not require phase control or measurement, which considerably simplifies

* Corresponding author: johannes.seelig@caesar.de

the experimental setup, and allows operating times of a few minutes. We validate the accuracy of our approach by showing different intensity distributions obtained after a glass diffuser and at the end of a multimode fiber.

The underlying approach is sketched in Fig. 1(a). In a first step, we generate a dataset consisting of pairs of binary illumination patterns displayed on the SLM and corresponding speckle patterns recorded with a CCD camera after transmission through the scatterer. These pairs of illumination and speckle patterns (typically on the order of 10000) are used to train the NNs as detailed in Methods, with the goal of inferring the relationship between the resulting scattered light distributions and the illumination patterns. We then feed the desired PSF into the trained NNs to predict the corresponding illumination pattern. This pattern is finally displayed on the SLM and the resulting light pattern is recorded with the camera. Each pattern, $\mathbf{C}(\mathbf{k})$, can be considered as a combination of plane waves with different wave vectors \mathbf{k} . This distribution of plane waves is modified by the scattering material through a function $F[\mathbf{C}(\mathbf{k})]$ in a deterministic way and results in the speckle pattern, \mathbf{S} , i.e $\mathbf{S} = F[\mathbf{C}(\mathbf{k})]$. After many trials, the NN learns an approximation of the function F needed to generate any light distribution after the scatterer.

The experimental setup is schematically shown in Fig. 1(b) and explained in detail in Methods. A laser beam is sent to the SLM, a high-speed digital micromirror device (DMD), which displays binary patterns of high and low intensity values (0s and 1s) with a frame rate of up to 22.7 kHz. We have tested our system, both with pseudo-random checkerboard-like patterns and with patterns obtained from Hadamard matrices. These patterns are imaged onto the back aperture of a microscope objective that focuses the light beam through the scatterer. A second identical microscope objective and a pair of lenses are used to collect and image the speckle patterns onto the CCD camera. Once the NN is trained, this setup allows real-time, single-shot light control through the scattering material, in a fashion similar to transmission matrix based approaches [11, 30, 49].

In Fig. 2 we demonstrate the ability of NNs to generate diffraction-limited Gaussian foci through a glass diffuser at different positions in the image plane with (a) a SLNN and (b) a CNN. Top images depict the NN architecture (see Methods for details); the first rows show the intensity distribution captured with the CCD camera, while the second and third rows display horizontal and vertical cross sections through the center of the focus. Insets and red-dashed lines show the position and shape of the desired focus. The images show an excellent agreement between the desired and recorded patterns with a signal-to-noise ratio > 10 both with the SLNN and the CNN.

To further prove the validity of our approach for controlling the light intensity distribution after the scatter we generated in Fig. 3 a variety of non-trivial shapes using SLNNs. Again, there is an excellent correspondence between the predicted (insets) and recorded patterns. We

here only use SLNNs for generating complex patterns. While CNNs have the advantage of being independent of assumptions about the underlying scattering process (such as linearity) and reduce the number of network parameters (by 80% for the two networks shown here), they need to be specifically trained for complex patterns. We note, however, that thanks to the high frame rate of the DMD (22.7 kHz), alternatively, any shape can be generated with high fidelity by painting it spot by spot, e. g. similar to approaches for trapping ultra cold atoms [50], as shown in Supplementary Figure 1 and in Supplementary Movies 1–6.

Our system is suited well to correct for scattering in materials with slow dynamics (on the order of minutes), such as optical fibers [51, 52]. In particular multimode optical fibers are ideal for applications in imaging and optogenetics, but modal dispersion and cross-talk distribute light into an apparently random speckle pattern. We therefore tested the performance of SLNNs for controlled light delivery through multimode fibers. In Fig. 4 a single focus is scanned with different paths across the field of view of the fiber (including a circle, a square, and a 5×5 array of points), demonstrating that SLNNs are able to precisely control light through optical fibers in a way suitable for scanning microscopy or optogenetics.

In summary, we have demonstrated that NNs can be used to efficiently shape light through scattering media. Our technique only requires binary intensity modulation and intensity measurements, which simplifies the setup and data analysis compared to approaches that also rely on phase information. Once the NNs are trained (which in our setup takes less than 5 minutes from recording the data to finishing training for the SLNNs and similar for fine-tuning the CNNs), this approach provides single-shot PSF engineering with high fidelity. We have demonstrated the ability of SLNNs and CNNs to focus and scan light through a glass diffuser and the ability of SLNNs to generate arbitrary light distributions, such as multiple foci, lines, letters, and numbers. We have further shown that SLNNs can focus and scan through multimode fibers.

SLNNs take advantage of the linearity of scattering (as does the transmission matrix approach) and therefore can generalize from speckle patterns to arbitrary light distributions. Multi-layer NNs in contrast need to be specifically designed and trained to generate a desired type of light distribution. At the same time, multi-layer NNs are more broadly applicable since no assumption about the underlying physical model (such as linearity of scattering) is made. Another advantage of CNNs compared to SLNNs is that they can efficiently reduce the dimensionality of the images through convolutional layers and lower the number of parameters required for training (by 80% compared to the SLNNs in our case).

The demonstrated approach could be extended to shape other properties of the light field such as its polarization or phase, thus increasing the level of control after the scatter [3]. Additionally, although we have used

monochromatic light in the reported experiments, our approach could also be used with pulsed light [53]. We believe that the simplicity, effectiveness and flexibility of the method presented here will make it suitable for many different applications where scattering needs to be controlled, such as optical trapping, biological imaging, optogenetic control or fiber-optical communication.

METHODS

Experimental setup

The laser beam ($\lambda = 640$ nm, power $P = 5$ mW; iBeamSmart, Toptica) is expanded with a telescope ($f_1 = 15$ mm, $f_2 = 150$ mm) and sent to the SLM. The SLM is a high-speed digital micromirror device (DMD, 768×1024 pixels, pixel size = $13.7 \mu\text{m}^2$; model V-7000 from Vialux) allowing binary amplitude modulation at a maximum frame rate of 22.7 kHz and is used to display binary pseudo-random checkerboard or Hadamard patterns with 64×64 macropixels extending over the central 768×768 pixels of the DMD. Two additional lenses ($f_3 = 200$ mm, $f_4 = 50$ mm) combined with a pinhole are used after the DMD to filter the maximum-intensity diffraction order mode and to demagnify and image the DMD onto the back aperture of the microscope objective (10X, 0.25 NA, Olympus). The objective focuses the light beam through the scatterer (a glass diffuser, Thorlabs DG20-120, and a step-index multimode fiber optic patch cable, Thorlabs M38L02) and a second identical microscope objective is used to collect the scattered light. Finally, a pair of lenses ($f_5 = 100$ mm, $f_6 = 75$ mm) in $2f$ configuration images the back aperture of the second microscope objective onto the CCD camera (acA640-750um, Basler), capturing images typically at 500 fps with resolution of 480×640 pixels (pixel size $4.8 \mu\text{m}^2$). Both microscope objectives and the scattering material are mounted on XYZ stages (omitted in the figure) for aligning the system and moving the sample to different positions, as well as for displacing the image plane axially. First, typically 10000 checkerboard patterns are uploaded to the internal memory of the DMD. Then, the projection of a pattern on the DMD triggers the frame capture of the CCD camera. The maximum frame rate of the DMD is 22.7 kHz and the maximum frame rate of the CCD camera is about 1000 fps at a resolution of 96×96 pixels, which allow us to record the whole sequence in about 10 s. We also note that our approach is valid for larger fields of view than those shown in the main figures ($20 \times 20 \mu\text{m}^2$, see Supplementary Information). The number of controlled optical modes used in the SLM can still be expanded by an order of magnitude for higher resolution applications.

Computer specifications

Our computer has a Linux-Ubuntu operating system, an Intel Xeon CPU E5-1620 v4 @ 3.50 GHz, 32Gb of DDR5 RAM memory, and a Nvidia Titan XP GPU possessing 3840 CUDA cores running at 1.60 GHz and with 12GB of GDDR5X memory running at over 11 Gbps.

Neural network design and performance

We use the Keras library [54] with the TensorFlow [55] back-end for GPU-accelerated neural network training. The networks are trained to map grayscale speckle images to the corresponding binary illumination patterns with a subset of the total dataset of image pairs (8000 pairs in our case) and tested on the previously not introduced data (the remaining 2000 pairs). Once the network is trained, we input the desired PSF and the output binary map is uploaded to the DMD for light control through the diffuser or fiber.

The SLNN we used is a single-layer perceptron, which is a network consisting of one fully connected layer followed by a non-linear activation function bounding the output to the 0-1 range. In principle, it can be represented as a matrix dot product, with bias addition and a sigmoid function applied element-wise to the resulting vector. We found that with the activation function applied per each individual element the model is prone to overfitting and does not make good generalizations. As a solution, we replaced the nonlinear activation function with a binarization function with a threshold common for the whole predicted pattern (mean value of the prediction) which results in a more robust model with better focus enhancement and faster training. The training time depends on the number of images used (8000 in our case), the batch size (number of images taken for each iteration of the training algorithm, 150 in our case), and the number of epochs (20 for the results presented here). With these parameters the single-layer perceptron requires less than 4 minutes for training, while the predicted patterns take about 1 s to be calculated.

In perceptron-like models a single fully-connected layer contains a large number of parameters (the product of input and output vector dimensions) which makes these models more demanding to train as the resolution of the illumination and speckle images and the memory demand increase. CNNs can efficiently reduce the number of trainable parameters and we used a model with three convolutional layers with 48 (9×9), 24 (5×5) and 12 (3×3) filters respectively, each succeeded by rectified linear unit (ReLU) activation and (2×2) max pooling operation, followed by a fully connected layer with 0.25 dropout rate. This configuration achieves a performance similar to the SLNN in controlling a single focal spot while having 20% of the SLNN's number of parameters.

As any deeper network, the CNN requires longer training time and a more extensive dataset. A workaround is

offered by the fine tuning technique: the convolutional layers are pretrained separately on a dataset of 40000 speckle images in an autoencoder. An autoencoder is a network trained to map its input to itself, however it contains a bottleneck - a lower dimensional middle layer (latent space) where a compressed representation of the data is learned. Our autoencoder has 3 convolutional layers as needed for the proposed CNN model and a symmetrical deconvolutional decoder. The training time largely varies with dataset size and speckle image resolution, and it is best to provide as much data as possible. Good training results were achieved after 20 minutes of training with 40000 samples sized 256×256 . The illumination-predicting CNN is then constructed from the pretrained encoder and an untrained dense output layer. During the training through backpropagation, predominantly the output layer is adjusted, while the convolutional layers are already initialized with adequate values to compress the speckle images and extract features. This allows to cut down the CNN training time to under 4 minutes while using the same 8000 image-pair dataset, comparable to the SLNN.

ACKNOWLEDGEMENTS

We thank Andres Flores for Python support and Bernd Scheiding for electronics support. We gratefully acknowl-

edge the support of NVIDIA Corporation with the donation of the Titan Xp GPU used for this research. This work was supported by the Max Planck Society and the Center of Advanced European Studies and Research (caesar).

AUTHOR CONTRIBUTIONS

A.T. performed the experiments and analyzed the data. I.V. designed the neural network analysis. A.T., I.V., and J.S. designed the project and wrote the manuscript.

COMPETING INTERESTS

The authors declare no competing financial interests.

[1] Ji, N. Adaptive optical fluorescence microscopy. *Nature Methods* **14**, 374–380 (2017).

[2] Booth, M. J. Adaptive optical microscopy: the ongoing quest for a perfect image. *Light: Science and Applications* **3**, e165 (2014).

[3] Rotter, S. & Gigan, S. Light fields in complex media: Mesoscopic scattering meets wave control. *Reviews of Modern Physics* **89**, 015005 (2017).

[4] Ruan, H. *et al.* Deep tissue optical focusing and optogenetic modulation with time-reversed ultrasonically encoded light. *Science Advances* **3**, eaao5520 (2017).

[5] Čižmár, T., Mazilu, M. & Dholakia, K. In situ wavefront correction and its application to micromanipulation. *Nature Photonics* **3**, 388–394 (2010).

[6] Čižmár, T. & Dholakia, K. Exploiting multimode waveguides for pure fibre-based imaging. *Nature Communications* **3**, 1027 (2012).

[7] Choi, Y. *et al.* Scanner-free and wide-field endoscopic imaging by using a single multimode optical fiber. *Physical Review Letters* **109**, 203901 (2012).

[8] Vellekoop, I. M. & Mosk, A. P. Focusing coherent light through opaque strongly scattering media. *Optics Letters* **32**, 2309–2311 (2007).

[9] Vellekoop, I. M. Feedback-based wavefront shaping. *Optics Express* **23**, 12189–12206 (2015).

[10] Horstmeyer, R., Ruan, H. & Yang, C. Guidestar-assisted wavefront-shaping methods for focusing light into biological tissue. *Nature Photonics* **9**, 563–571 (2015).

[11] Popoff, S. M. *et al.* Measuring the transmission matrix in optics: An approach to the study and control of light propagation in disordered media. *Physical Review Letters* **104**, 100601 (2010).

[12] Conkey, D. B., Caravaca-Aguirre, A. M. & Piestun, R. High-speed scattering medium characterization with application to focusing light through turbid media. *Optics Express* **20**, 1733–1740 (2012).

[13] Drémeau, A. *et al.* Reference-less measurement of the transmission matrix of a highly scattering material using a dmd and phase retrieval techniques. *Optics Express* **23**, 11898–11911 (2015).

[14] Forbes, A., Dudley, A. & McLaren, M. Creation and detection of optical modes with spatial light modulators. *Adv. Opt. Photon* **8**, 200–227 (2016).

[15] Turtaev, S. *et al.* Comparison of nematic liquid-crystal and dmd based spatial light modulation in complex photonics. *Optics Express* **25**, 29874–29884 (2017).

[16] Leonardo, R. D. & Bianchi, S. Hologram transmission through multi-mode optical fibers. *Optics Express* **19**, 247–254 (2011).

[17] Kim, D. *et al.* Toward a miniature endomicroscope: pixelation-free and diffraction-limited imaging through a fiber bundle. *Optics Express* **39**, 1291–1294 (2014).

[18] Yoon, J. *et al.* Optogenetic control of cell signaling pathway through scattering skull using wavefront shaping. *Scientific Reports* **3**, 13289 (2015).

[19] Wang, D. *et al.* Focusing through dynamic tissue with millisecond digital optical phase conjugation. *Optica* **2**,

728–735 (2015).

[20] Liu, Y., Lai, P., Ma, C., Xu, X. & andLihong V. Wang, A. A. G. Optical focusing deep inside dynamic scattering media with near-infrared time-reversed ultrasonically encoded (true) light. *Nature Communications* **6**, 5904 (2015).

[21] Cui, M. & Yang, C. Implementation of a digital optical phase conjugation system and its application to study the robustness of turbidity suppression by phase conjugation. *Optics Express* **18**, 3444–3455 (2010).

[22] Hsieh, C.-L., Pu, Y., Grange, R., Laporte, G. & Psaltis, D. Imaging through turbid layers by scanning the phase conjugated second harmonic radiation from a nanoparticle. *Optics Express* **18**, 20723–20731 (2010).

[23] Wang, Y. M., Judkewitz, B., DiMarzio, C. A. & Yang, C. Deep-tissue focal fluorescence imaging with digitally time-reversed ultrasound-encoded light. *Nature Communications* **3**, 928 (2012).

[24] Hillman, T. R. *et al.* Digital optical phase conjugation for delivering two-dimensional images through turbid media. *Scientific Reports* **3**, 1909 (2013).

[25] Liu, Y., Ma, C., Shen, Y., Shi, J. & Wang, L. V. Focusing light inside dynamic scattering media with millisecond digital optical phase conjugation. *Optica* **4**, 280–288 (2017).

[26] Mosk, A. P., Lagendijk, A., Lerosey, G. & Fink, M. Controlling waves in space and time for imaging and focusing in complex media. *Nature Photonics* **6**, 283–292 (2012).

[27] Tanga, J., Germain, R. N., & Cui, M. Superpenetration optical microscopy by iterative multiphoton adaptive compensation technique. *Proceedings of the National Academy of Sciences* **129**, 8434–8439 (2012).

[28] Blochet, B., Bourdieu, L. & Gigan, S. Focusing light through dynamical samples using fast continuous wavefront optimization. *Optics Letters* **42**, 4994–4997 (2017).

[29] Popoff, S., Lerosey, G., Fink, M., Boccara, A. C. & Gigan, S. Image transmission through an opaque material. *Nature Communications* **1**, 81 (2010).

[30] Boniface, A., Mounaix, M., Blochet, B., Piestun, R. & Gigan, S. Transmission-matrix-based point-spread-function engineering through a complex medium. *Optica* **4**, 54–59 (2017).

[31] Metzler, C. A. *et al.* Coherent inverse scattering via transmission matrices: Efficient phase retrieval algorithms and a public dataset. In *2017 IEEE International Conference on Computational Photography (ICCP)*, 1–16 (2017).

[32] Jordan, M. I. & Mitchell, T. M. Machine learning: Trends, perspectives, and prospects. *Science* **349**, 255–260 (2015).

[33] LeCun, Y., Bengio, Y. & Hinton, G. Deep learning. *Nature* **521**, 436–444 (2015).

[34] Waller, L. & Tian, L. Machine learning for 3d microscopy. *Nature* **523**, 416–417 (2015).

[35] Deans, C., Griffin, L. D., Marmugi, L., & Renzoni, F. Machine learning based localization and classification with atomic magnetometers. *Physical Review Letters* **120**, 033204 (2018).

[36] Kamilov, U. S. *et al.* Learning approach to optical tomography. *Optica* **2**, 517–522 (2015).

[37] Sinha, A., Li, J. L. S. & Barbastathis, G. Lensless computational imaging through deep learning. *Optica* **4**, 1117–1125 (2017).

[38] Rivenson, Y. *et al.* Deep learning microscopy. *Optica* **4**, 1437–1443 (2017).

[39] Nehme, E., Weiss, L. E., Michaeli, T., & Shechtman, Y. Deep-storm: Super resolution single molecule microscopy by deep learning. *arXiv preprint arXiv:1801.09631v1* (2018).

[40] Conkey, D. B., Brown, A. N., Caravaca-Aguirre, A. M. & Piestun, R. Genetic algorithm optimization for focusing through turbid media in noisy environments. *Journal of Optics* **20**, 4840–4849 (2012).

[41] Zhang, X. & Kner, P. Binary wavefront optimization using a genetic algorithm. *Journal of Optics* **17**, 125704 (2014).

[42] Tehrani, K. F., Xu, J., Zhang, Y., Shen, P. & Kner, P. Adaptive optics stochastic optical reconstruction microscopy (ao-storm) using a genetic algorithm. *Optics Express* **23**, 13677–13692 (2015).

[43] Zhang, B. *et al.* Focusing light through strongly scattering media using genetic algorithm with sbr discriminant. *Journal of Optics* **20**, 025601 (2017).

[44] Ando, T., Horisaki, R. & Tanida, J. Speckle-learning-based object recognition through scattering media. *Optics Express* **23**, 33902–33910 (2015).

[45] Horisaki, R., Takagi, R. & Tanida, J. Learning-based imaging through scattering media. *Optics Express* **24**, 13738–13743 (2016).

[46] Horisaki, R., Takagi, R. & Tanida, J. Learning-based focusing through scattering media. *Applied Optics* **56**, 4358–4362 (2017).

[47] Li, S., Deng, M., Lee, J., Sinha, A. & Barbastathis, G. Imaging through glass diffusers using densely connected convolutional networks. *arXiv preprint arXiv:1711.06810v1* (2017).

[48] Lyu, M., Wang, H., Li, G. & Situ, G. Exploit imaging through opaque wall via deep learning. *arXiv preprint arXiv:1711.06810v1* (2017).

[49] Damien Loterie, D. P. C. M., Salma Farahi. Complex pattern projection through a multimode fiber (2015).

[50] Henderson, K., Ryu, C., MacCormick, C. & Boshier, M. G. Experimental demonstration of painting arbitrary and dynamic potentials for bose-einstein condensates. *New Journal of Physics* **11**, 043030 (2009).

[51] Caravaca-Aguirre, A. M. & Piestun, R. Single multimode fiber endoscope. *Optics Express* **25**, 1656–1665 (2017).

[52] Ohayon, S., Caravaca-Aguirre, A. M., Piestun, R. & DiCarlo, J. J. Deep brain fluorescence imaging with minimally invasive ultra-thin optical fibers. *arxiv preprint arXiv:1703.07633* (2017).

[53] Sun, B. *et al.* Four-dimensional light shaping: manipulating ultrafast spatiotemporal foci in space and time. *Light: Science and Applications* **7**, 17117 (2018).

[54] Chollet, F. *et al.* Keras. <https://github.com/keras-team/keras> (2015).

[55] Abadi, M. *et al.* TensorFlow: Large-scale machine learning on heterogeneous systems (2015). URL <http://tensorflow.org/>.

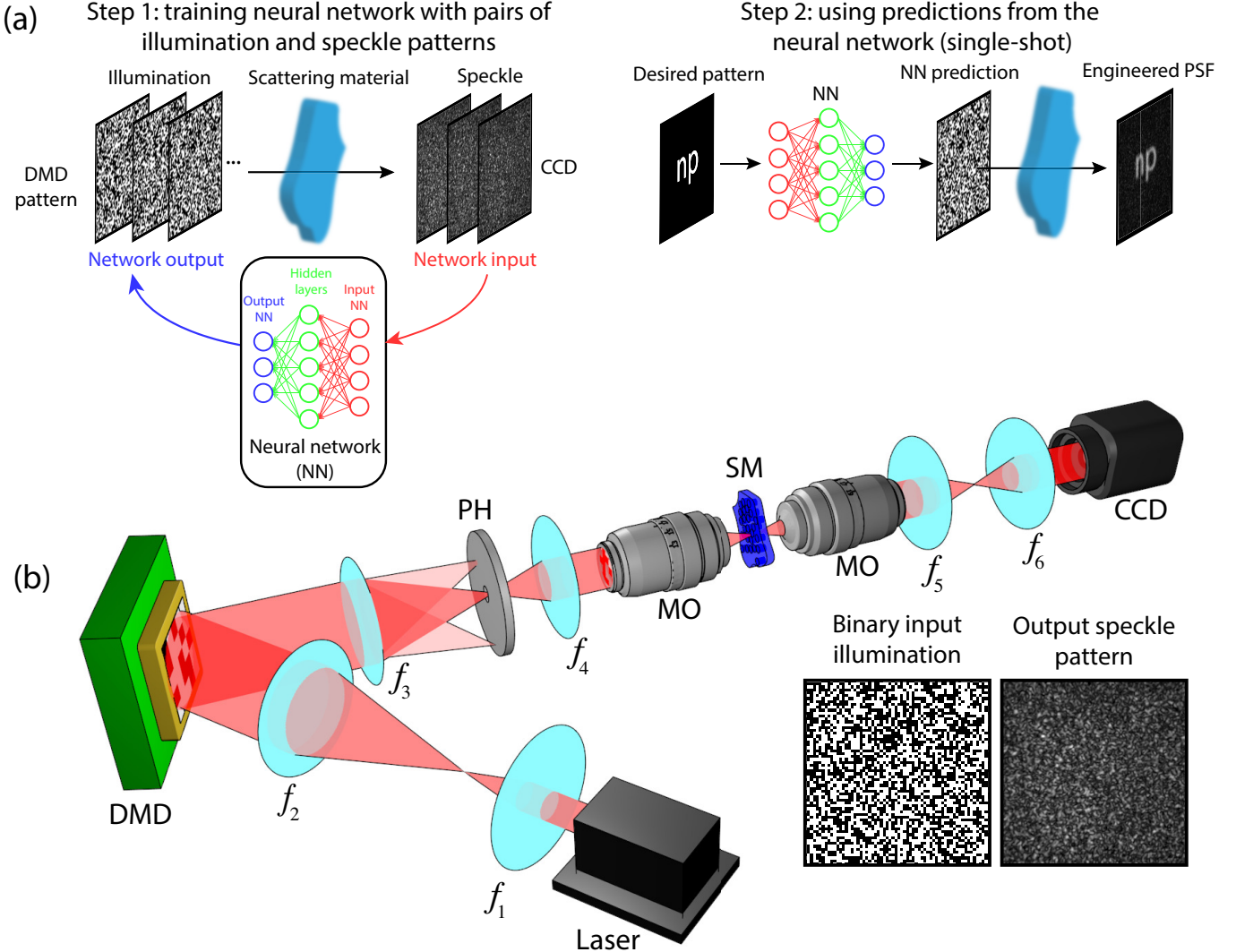


FIG. 1. (a) Approach for light control through scattering media with NNs. A NN is trained with pairs of illumination and speckle patterns, using the speckle as input of the network and the illumination as output. Once the NN is trained, it is used to predict the illumination necessary to generate a target pattern after the scattering material. The predicted illumination is subsequently sent through the material resulting in the desired light pattern. **(b) Experimental setup.** An expanded laser beam at 640 nm illuminates the SLM (in our case a DMD) allowing for binary modulation of the light beam. After filtering the maximum-intensity diffraction order with a pair of lenses and a pinhole (PH), the DMD pattern is sent to the scattering material (SM) with a 10 \times microscope objective (MO, NA = 0.25). An additional identical objective is used to collect the transmitted light and is imaged onto a CCD camera with an additional pair of lenses. Both objectives and the sample are mounted on XYZ translation stages (omitted in the figure).

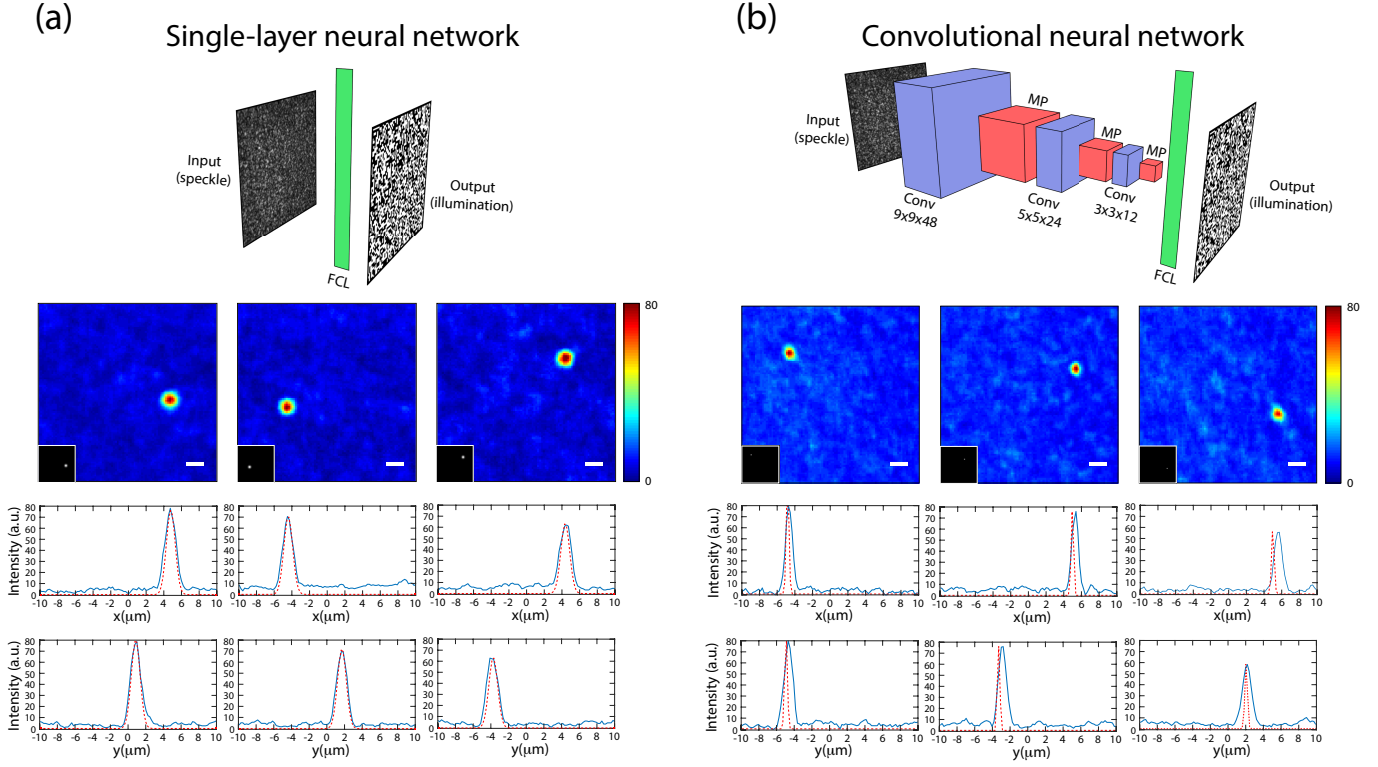


FIG. 2. Focusing with neural networks. Intensity distributions (first row) and intensity profiles through the foci along horizontal (second row) and vertical (third row) directions of Gaussian beams obtained at different positions after training (a) the SLNN and (b) the CNN. Red-dashed lines (---) are the theoretical predictions of intensity distribution normalized to the corresponding experimental result. Scale bars = 2 μ m. FCL: fully-connected layer; Conv $n \times m \times p$: convolutional layer of p kernels with dimensions $n \times m$; MP: max pooling operation reducing the previous element size. Color bars: intensity (a.u.).

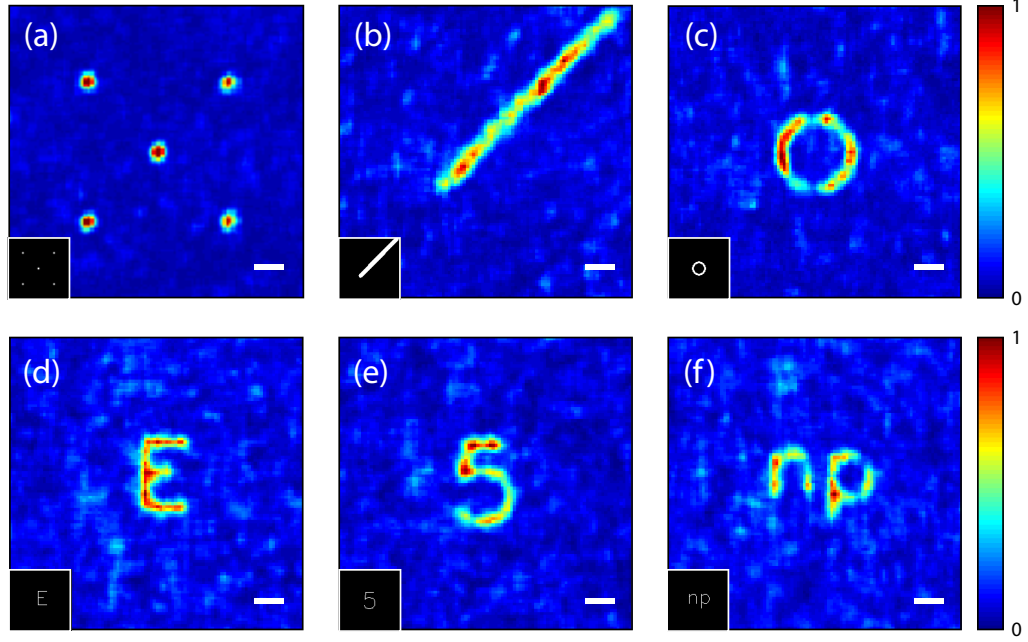


FIG. 3. **Light control through a glass diffuser with a SLNN.** Normalized intensity patterns obtained after the glass diffuser with the SLNN: (a) five Gaussian foci; (b) a line at 45° ; (c) a ring; (d) the letter "E"; (e) the number "5"; and (f) the letters "np". Insets show the desired light distribution. Scale bars = $2 \mu\text{m}$. Color bars: intensity (a.u.) normalized for each image.

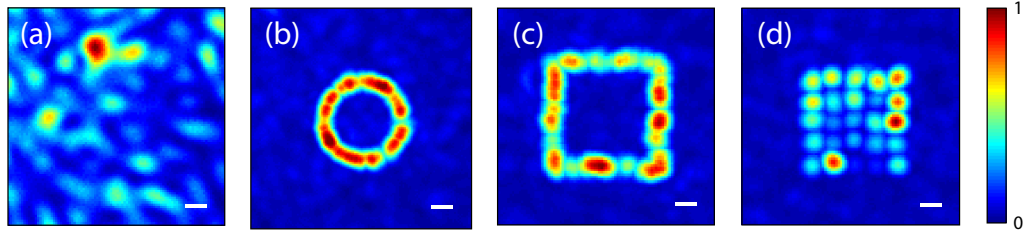


FIG. 4. **Neural networks focus light through multimode fibers.** Normalized transverse intensity distributions of the light field after a multimode fiber when (a) no correction is applied and when a single focus is scanned along (b) a circle, (c) a square, and (d) an array of 5×5 points. Scale bars = $2.3 \mu\text{m}$. Color bar: intensity (a.u.) normalized for each image.

SUPPLEMENTARY INFORMATION: LIGHT CONTROL THROUGH SCATTERING MEDIA WITH NEURAL NETWORKS

Pattern generation by scanning a focus at high frequency

Since neural networks can generate single foci with high fidelity, one can take advantage of the fast operation of the DMD (22.7 kHz) to obtain any transverse intensity distribution after the scatter by scanning a single spot (or multiple spots) at high speed. This is shown in Supplementary Figure 5 for a single focus tracing out (a/d) a circle, (b/e) a square, and (c/f) a square grid consisting of 128/96, 256/256, and 25/25 scanning positions, respectively, both for the SLNN (first row) and the CNN (second row). Supplementary Movies 1–6 show projections of these sequences recorded at a speed of 500 Hz (the fastest allowed by our CCD camera). Note that for the DMD operating at full speed, i.e. without restrictions imposed by the camera, a sequence composed of 96 focus positions projecting a certain pattern will result in a pattern projection frame rate higher than 200 Hz.

Light control over different fields of view

In the main text we have shown the ability of NNs to shape light through disordered media within a field of view of $20 \times 20 \mu\text{m}^2$ imaged onto 96×96 pixels on the CCD camera. However, the presented method performs similarly for other fields of view, as shown in Supplementary Figure 6 for the case of the glass diffuser, with 64×64 macropixels displayed on the DMD controlled with the SLNN. In all cases, the experimental setup is the same as the one shown in the main text and the only difference is the resolution of the images captured with the CCD camera and used to train the SLNN. Note that the illumination resolution additionally impacts the quality of light shaping through the diffuser (in agreement with previous reports, see e.g. Ref. [8]).

Training performance of SLNN

Although neural networks are capable of predicting the illumination patterns necessary for light control through scattering media, there are multiple variables affecting the efficiency of the training. Here, we discuss the impact of the size of the dataset used for training. In Supplementary Figure 7 we plot the mean-square error (MSE) between the predicted illuminations after training the single-layer neural network and a set of 100 original illuminations that were not included in the training. The analysis is performed for different sizes of the dataset (ranging from 800 pairs to 8000 pairs) and different illumination sizes: 64×64 (red), 32×32 (green), and 16×16 (blue). As an illustration of the training performance, we

have included an example of original illumination and corresponding predictions obtained when 1600, 3200, 4800, 6200, and 8000 pairs are used (16×16 case). As expected, the lower the size of the illumination pattern, the higher the MSE.

Supplementary Movie Captions

Note: for all movies intensity is normalized for each frame.

Supplementary Movie 1

A single focus generated with a SLNN is scanned at 128 different positions forming a circle through a glass diffuser at a projection rate of 500 Hz.

Supplementary Movie 2

A single focus generated with a SLNN is scanned at 256 different positions forming a square through a glass diffuser at a projection rate of 500 Hz.

Supplementary Movie 3

A single focus generated with a SLNN is scanned at 25 different positions forming a grid through a glass diffuser at a projection rate of 500 Hz.

Supplementary Movie 4

A single focus generated with a CNN is scanned at 96 different positions forming a circle through a glass diffuser at a projection rate of 500 Hz.

Supplementary Movie 5

A single focus generated with a CNN is scanned at 256 different positions forming a square through a glass diffuser at a projection rate of 500 Hz.

Supplementary Movie 6

A single focus generated with a CNN is scanned at 25 different positions forming a grid through a glass diffuser at a projection rate of 500 Hz.

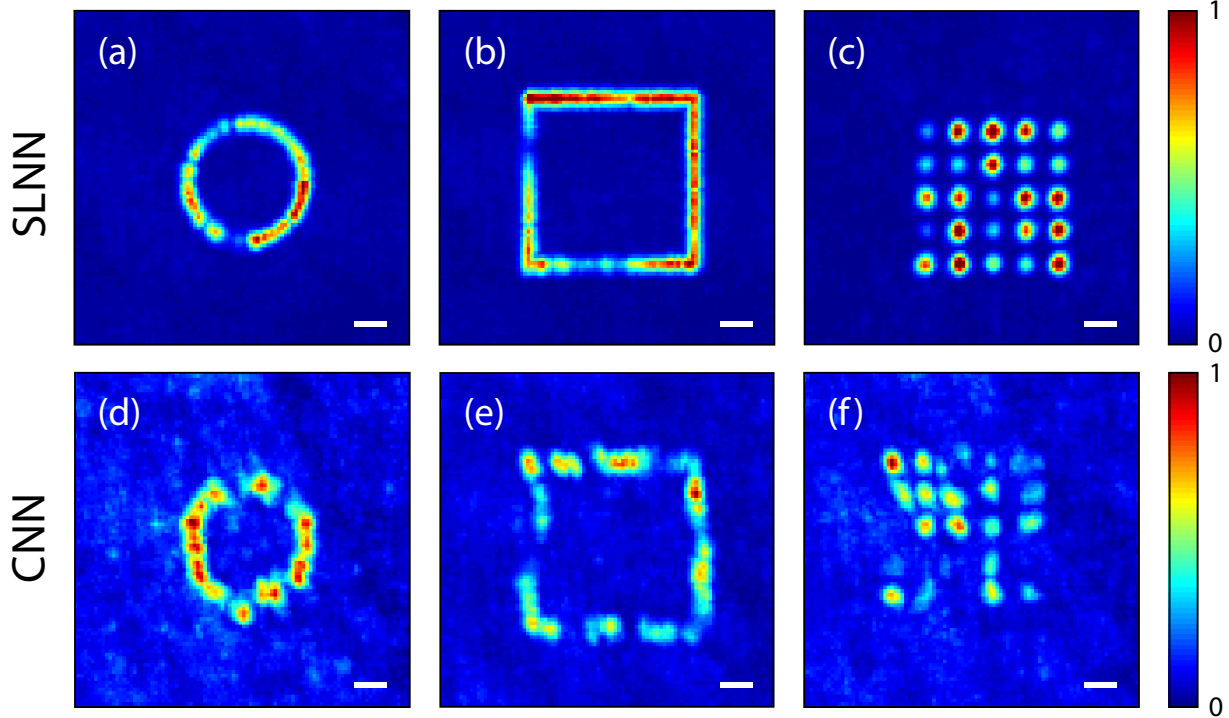


FIG. 5. Single-focus scanning allows time-averaged pattern projection. Patterns obtained when a single focus is scanned following (a/d) a circle (128/96 scanning points), (b/e) a square (256/256 scanning points), and (c/f) a grid of 5×5 points with the SLNN (first row) and the CNN (second row). Color bars: intensity (a.u.) normalized for each image.

Supplementary Movie 7

A single focus generated with a SLNN is scanned at 96 different positions forming a circle through a multimode fiber at a projection rate of 500 Hz.

Supplementary Movie 8

A single focus generated with a SLNN is scanned at 256 different positions forming a square through a multimode fiber at a projection rate of 500 Hz.

Supplementary Movie 9

A single focus is scanned at 25 different positions forming a grid through a multimode fiber at a projection rate of 500 Hz.

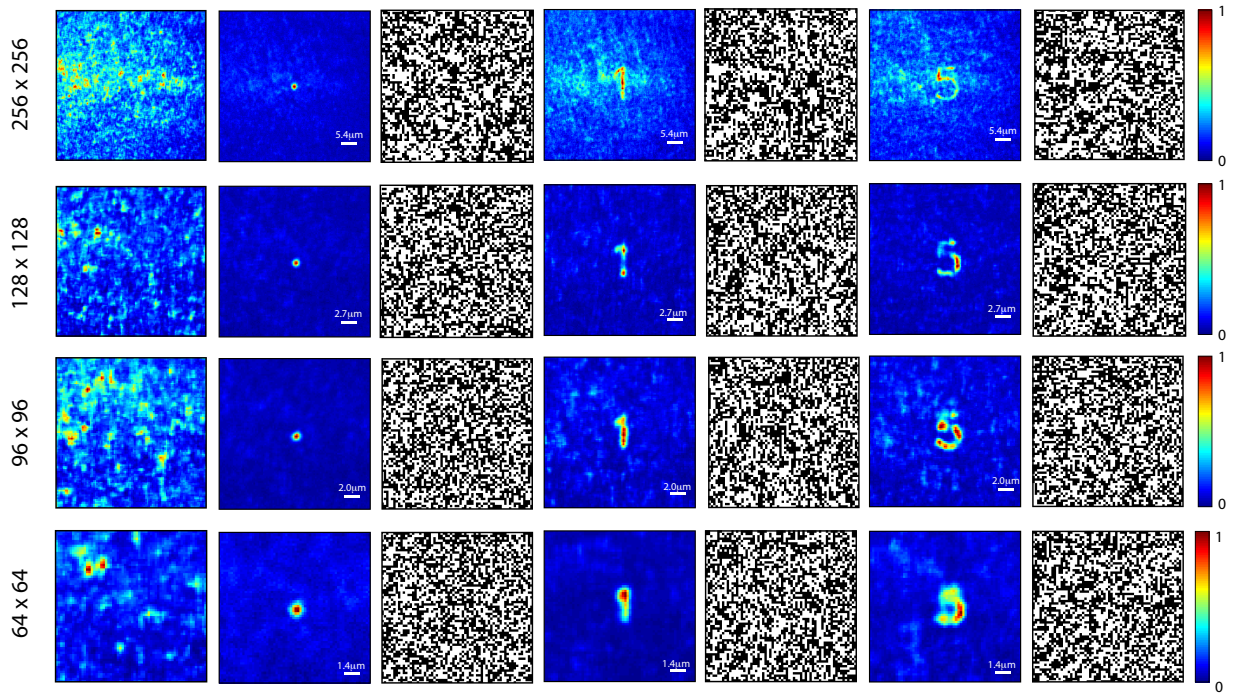


FIG. 6. Light control over different fields of view. Normalized transverse intensity distributions of an example of speckle pattern (first column), a single focus (second column), the number “1” (fourth column), and the number “5” (6th column) for different fields of view: 256×256 pixels (first row), 128×128 pixels (second row), 96×96 pixels (third row), and 64×64 pixels (last row). Columns number 3, 5, and 7 are the actual DMD patterns used to generate the light distributions from columns number 2, 4, and 6, respectively. Color bars: intensity (a.u.) normalized for each image.

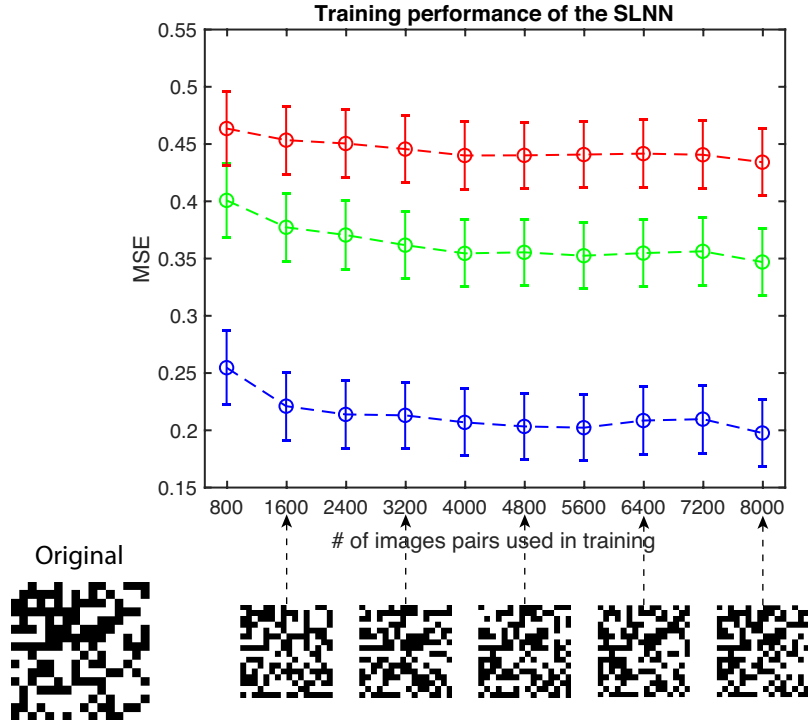


FIG. 7. **Training performance of SLNN.** Mean-square error (MSE) between the predicted and original illumination patterns for the single-layer neural network for different sizes of the dataset. Red-, green-, and blue-dashed curves correspond to illumination sizes of 64×64 , 32×32 , and 16×16 , respectively. Insets below show the the predicted illumination at different stages of the training for the 16×16 case. Scale bars = $2 \mu\text{m}$.